Processing effects on the composition and dielectric properties of hydrothermally derived $Ba_xSr_{(1-x)}TiO_3$ thin films

Mark A. McCormick, Ryan K. Roeder,[a] and Elliott B. Slamovich
School of Materials Engineering, Purdue University, West Lafayette, Indiana 47907-1289

(Received 1 November 2000; accepted 2 February 2001)

Polycrystalline $Ba_xSr_{(1-x)}TiO_3$ (BST) thin films were processed on Pt-coated glass substrates at temperatures below 100 °C by reacting TiO_2 films in alkaline solutions containing Ba^{2+} and/or Sr^{2+}. The TiO_2 was deposited by spin-casting a titanium metalorganic precursor onto Pt-coated glass substrates, followed by pyrolysis in air at 400 °C. Film stoichiometry deviated from the initial solution composition, with a preferred incorporation of Sr^{2+} into the perovskite lattice. The BST thin films had dielectric constants ranging from 100 to 185 and dielectric loss values below 0.25. Capacitance–voltage and current–voltage relationships were examined to determine the effect of phase stoichiometry and processing route on dielectric properties.

I. INTRODUCTION

The properties of dielectric and ferroelectric powders and thin films make them attractive for a variety of applications including the following: nonvolatile ferroelectric memories; microwave devices; dynamic random access memories (DRAMs); multilayer capacitors; microelectromechanical systems (MEMS); pyroelectric detectors; piezoelectric actuators; optoelectronic devices.[1–9] For example, random access memories (RAM) using SiO_2/Si_3N_4 dielectrics have matured from planar capacitors into complicated three-dimensional structures (stack and trench geometries) in order to increase the capacitor area as memory requirements have grown. However, application of high dielectric constant materials like $Ba_xSr_{(1-x)}TiO_3$ (BST) allow more charge storage per unit area, further decreasing the size of memory cells while facilitating the return to planar geometries. Furthermore, planar design allows the use of less complicated and less costly fabrication processes.

High dielectric constants, low leakage currents, and high dielectric breakdown strengths are characteristic of perovskite materials such as BST. For applications as a capacitor (e.g., DRAM), BST must exhibit a sufficiently large polarizability and a sufficiently low leakage current such that the capacitor does not discharge before it is refreshed. Further, since devices are generally run under an applied dc bias voltage, the effects of electric fields on the dielectric properties cannot be ignored. Therefore, the influence of processing parameters on the interactions among film composition, microstructure, and properties must be assessed to ensure device reliability.

Processing routes to BST, including sputtering, laser ablation, MOCVD, and chemical solution deposition (CSD), generally require deposition temperatures or heat treatments in excess of 500 °C.[9–13] In contrast, hydrothermal processing provides a low-temperature route (<100 °C) to synthesize crystalline ceramics in an aqueous medium. Control over hydrothermal solution conditions, such as composition, pH, and temperature, is critical to ensure the stability of the desired phase,[14] as well as to control the microstructure and composition of the resulting powder or thin film.[15–18] For example, Roeder and Slamovich studied the formation of BST powders processed at 80 °C by reacting nano-sized TiO_2 powders in alkaline, aqueous solutions of $BaCl_2$, $SrCl_2$, and NaOH.[19] In all cases, Sr^{2+} was more readily incorporated into the BST powders than Ba^{2+}, the extent varying systematically with the processing conditions.

In the present study, a method similar to that used to synthesize BST powders[19] was used to produce BST thin films with a range of compositions. A titanium metalorganic liquid precursor was first pyrolyzed to produce a dense TiO_2 film, which was subsequently reacted in alkaline aqueous solutions containing Ba^{2+} and Sr^{2+}. This study had two main objectives. The first was to determine if the preferred incorporation of Sr^{2+} observed for BST powders was also observed in hydrothermally derived thin films. To this end, BST thin films were processed under conditions similar to those used in the BST powder study. The second objective was to characterize

[a]Present address: Department of Orthopedic Surgery, Indiana University Medical Center, Indianapolis, IN 46202.

the dielectric properties of the hydrothermally derived BST thin films with and without an applied bias voltage. To this end, the processing conditions were modified to achieve dense, continuous films suitable for dielectric characterization.

II. EXPERIMENTAL PROCEDURE

BST thin films were processed using titanium dimethoxy dineodecanoate (TDD) synthesized by the method described by Shaikh and Vest.[20] TDD was chosen for the Ti metalorganic precursor film because of a high resistance to cracking during drying[21] relative to other Ti metalorganic precursors.[15,22] Glass substrates were coated with an approximately 0.1-μm-thick layer of Pt by dc sputtering (Hummer VI, Anatech, Ltd., Alexandria, VA). Pt was the chosen electrode material for its large work function, which creates a large potential barrier between the film and the electrode, thereby minimizing capacitor leakage during electrical property measurements.[23] TDD was diluted with *p*-xylene to a viscosity of approximately 5×10^{-3} Pa s and pipetted onto the metallized substrate. Spin-coating was carried out at 8000 rpm for 20 s, yielding TDD precursor films in the range 0.4–0.5-μm average thickness. The TDD film was then pyrolyzed in air at 400 °C for 20 min, after which a second TDD layer 0.4–0.5-μm thick was applied and pyrolyzed. Layering was necessary to avoid precursor cracking during firing and to provide sufficient Ti for conversion to a continuous BST film. The final thickness of the bilayer TiO_2 film was approximately 0.2 μm as determined by surface profilometry and cross-section scanning electron microscopy (SEM).

Alkaline aqueous solutions containing Ba^{2+} and Sr^{2+} were prepared by first boiling deionized water for at least 20 min to remove dissolved carbon dioxide. The water was maintained at 80 °C under moderate stirring while adding the appropriate amounts of reagent grade $BaCl_2 \cdot 2H_2O$ (EM Science, Gibbstown, NJ), $SrCl_2 \cdot 6H_2O$ (Aldrich Chemical Co., Inc., Milwaukee, WI), and NaOH (Mallinckrodt Chemical Inc.) or $Ba(OH)_2 \cdot 8H_2O$ (Mallinckrodt Chemical Inc., Paris, KY) and $Sr(OH)_2 \cdot 8H_2O$ (Aldrich Chemical Co., Inc.). Solutions of mixed chlorides were used to reproduce processing conditions previously reported for BST powder synthesis.[19] Solutions of mixed hydroxides were used to avoid the potentially adverse effects of Na^+ or Cl^- contamination on dielectric properties. The waters of hydration of the Ba^{2+} and Sr^{2+} sources were taken into account when calculating the volume of water and mass of chlorides required for a desired molarity. The total concentration of Ba^{2+} and Sr^{2+} cations in solution ($[Ba^{2+}] + [Sr^{2+}]$) was 0.4 and 0.5 M for solutions of mixed chlorides and hydroxides, respectively. After dissolution of the reagents, the solutions were filtered through a Buchner funnel to remove any precipitates. The solutions were sealed in polyethylene bottles and stored in an oven at 80 °C.

The pyrolyzed TiO_2 films were reacted for 36 h in Ba^{2+}- and Sr^{2+}-containing solutions of mixed chlorides and hydroxides at 80 and 90 °C, respectively. The total concentration of Ba^{2+} and Sr^{2+} initially in solution was kept constant, while the mole fraction of Ba^{2+} was varied from 0 to 1.0. The experimental parameters were kept as near the previously reported BST powder synthesis conditions[19] as possible. The only significant exception was the initial ratio of Ba^{2+} and Sr^{2+} in solution relative to Ti, which was much larger (approximately a factor of 1000) due to the small amount of Ti in the precursor film. After immersion of the substrates in the reaction solution, the polyethylene bottles were backfilled with Ar, sealed, and placed in a preheated forced convection oven for reaction. After reaction, bottles were transferred into a nitrogen atmosphere glove box (Kewaunee Scientific Engineering, Adrian, MI) to avoid formation of $BaCO_3$ upon removal from the solution. The films were removed from solution and immediately rinsed in a solution of deionized water adjusted to pH = 12 using NH_4OH (Mallinckrodt Chemical Inc.), followed by rinsing in ethanol (200-proof, McCormick Distilling Co., Inc.). The washing solutions were warm, having been stored in an oven at 80 °C during the reaction. The films were removed from the glovebox while in the ethanol wash and removed from the ethanol while blow-drying with air.

X-ray diffraction (XRD) was used for phase identification and quantitative compositional analysis. Powder diffraction (D500, Siemens Analytical X-ray Instruments Inc., Karlsruhe, Germany) was performed using Cu Kα radiation ($\lambda = 1.54$ Å). All BST thin films were examined over 20–60° 2θ at 10°/min, 20–35° 2θ at 1.2°/min, and 30–34° 2θ at 0.2°/min. Lattice parameters were determined from the (110) peak, fitting the data using a split Pearson VII function.[24] The composition of BST thin films was measured from a linear fit to the lattice parameters of the pure $BaTiO_3$ and $SrTiO_3$ films using Vegard's law. These measurements were confirmed by separate composition measurements using wavelength-dispersive-spectroscopy (WDS) (SX-50, Cameca Instruments Co., Courbevoie, France). Scanning electron microscopy (SEM) (JSM-35CF, JEOL Ltd., Akishima, Japan) was used to examine the microstructure and determine the film thickness from film cross sections. The thin-film grain size was measured from the breadth of the (110) BST reflection using the Scherrer equation and from stereological analysis of SEM images using the line-intercept method.

Planar capacitors were assembled using photolithography to sputter 10^4 μm^2 Pt electrodes onto the film surface. The capacitance and dielectric loss (tan δ) were measured over the frequency range 10 kHz to 10 MHz

using a Hewlett-Packard 4275A LCR (Palo Alto, CA) meter. All reported values for the dielectric constant and tan δ were measured at 10 kHz. After the dielectric properties were recorded at room temperature for the as-formed films, the films were heated in air to 200 °C for 30 min and the properties were measured as a function of temperature over the range 25 to 200 °C. Capacitance as a function of applied voltage (*C–V*) was measured using the LCR meter in combination with a Keithley 238 Source-Measurement Unit (Keithley Instuments, Inc., Cleveland, OH), the latter used to apply the dc voltage across the sample capacitor. Dc voltages over the range −8 to +8 V (corresponding to fields of ±170 kV/cm) with a step size of 0.5 V were used, and a constant ac voltage from the LCR meter was applied at a frequency of 10 kHz with amplitude 0.01 V. Dc leakage current as a function of applied voltage (*I–V*) was measured using the Keithley 238 to apply a staircase series of voltage steps as described by Dietz and Waser[25] and to measure the resulting current across the capacitor. Dc voltages over the range −14 to +14 V with a step size of 0.25 V were used. The leakage current was measured 1.0 s after applying the voltage to account for polarization currents.

III. RESULTS AND DISCUSSION

A. Thin-film microstructure and composition

The effects of the mole fraction of Ba^{2+} and Sr^{2+} initially in solution were examined by processing BST thin films at 90 °C for 36 h in aqueous solutions of $Ba(OH)_2$ and $Sr(OH)_2$. The mole fraction of Ba^{2+} and Sr^{2+} cations initially in solution was varied from 0.0 to 1.0, maintaining a fixed total concentration of Ba^{2+} and Sr^{2+} at 0.5 M. Plan-view and fractured cross-sectional SEM micrographs indicated that films were continuous (Fig. 1). The thin-film thickness was typically approximately 0.25 μm. XRD patterns revealed the formation of single-phase cubic BST solid solutions and minor amounts of carbonate contamination (Fig. 2). The absence of anatase TiO_2 reflections in XRD and a 1:1 molar ratio of Ba + Sr to Ti measured by WDS (Table I) suggest that the TiO_2 precursor film reacted to completion.

The film grain size depended on the solution composition, ranging from approximately 90 nm for $SrTiO_3$ to 180 nm for $BaTiO_3$ (Fig. 3). The grain size of Sr-rich BST films displayed little variation with increasing Ba content until approximately $Ba_{0.50}Sr_{0.50}TiO_3$. Between $Ba_{0.50}Sr_{0.50}TiO_3$ and $Ba_{0.70}Sr_{0.30}TiO_3$ the films exhibited a twofold increase in grain size. These results are similar to observations of BST powders in which the Ba-rich and Sr-rich BST particles ranged in size from 50 to 100 nm and 20 to 30 nm, respectively.[19] Grain size calculations using the Scherrer formula and the line-intercept method were in close agreement, suggesting that the grains in Fig. 1 were single crystals rather than composed of polycrystalline domains.

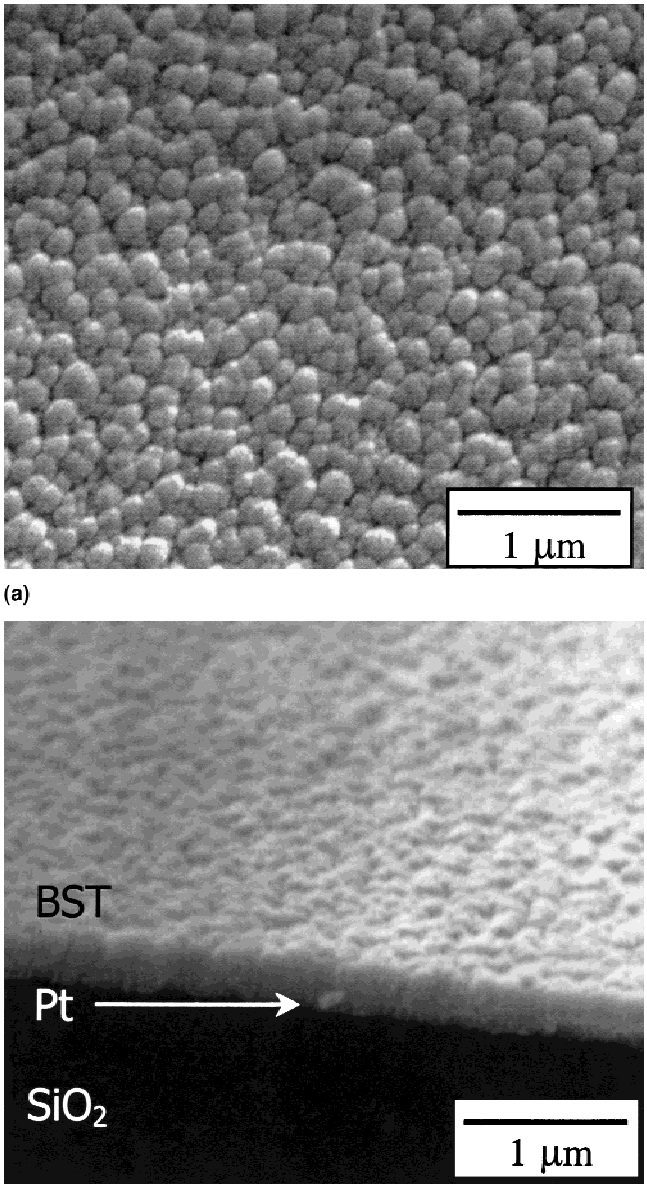

FIG. 1. (a) Plan-view and (b) cross-sectional SEM micrograph of $Ba_{0.20}Sr_{0.80}TiO_3$ thin film processed at 90 °C for 36 h using an aqueous solution of 0.25 M $Ba(OH)_2$ and 0.25 $Sr(OH)_2$.

The composition of BST thin films was determined by XRD using the (110) reflection (Fig. 4). As the mole fraction of Ba^{2+} in solution varied from 1.0 to 0.0, the (110) reflection for BST shifted from $BaTiO_3$ toward $SrTiO_3$. The lattice parameters of the hydrothermally derived $BaTiO_3$ and $SrTiO_3$ films were used as end points and were connected by a straight line assuming Vegard's law (Fig. 5). The composition of each BST film was then estimated using the lattice parameter measured from the

(110) reflection and the linear fit between the $BaTiO_3$ and $SrTiO_3$ end points. The validity of Vegard's law was assessed by measuring the composition of selected films using WDS. Typical WDS data are shown in Table I. Note that the x-ray signal from the BST thin films in WDS accounted for only 25–30% of the total intensity, with the remainder of the signal coming from the bottom Pt electrode and the glass substrate. Figure 5 plots the lattice parameters measured for BST thin films versus the film composition determined using both Vegard's law and WDS. For both sets of data, the lattice parameter is determined from the position of the (110) reflection. The "WDS" data obtain the Ba mole fraction by direct measurement, while the "XRD" data are obtained by a linear interpolation between pure $BaTiO_3$ and pure $SrTiO_3$ consistent with Vegard's law. The difference in film composition obtained by the two approaches was less than 4% and indicates that the film composition may be reliably calculated from XRD data using Vegard's law. Finally, note that JCPDS standards are also shown in Fig. 5 for comparison, but were not useful for composition measurements because hydrothermally derived films and powders present a consistently larger lattice parameter than films and powders processed by conventional high-temperature fabrication methods (Fig. 5). This discrepancy is most likely due to the presence of adsorbed hydroxyl ions in hydrothermally derived materials.[26,27]

Figure 6 shows the Ba^{2+} mole fraction in the BST product (*y*-axis) resulting from an initial Ba^{2+} mole fraction in the reaction solution (*x*-axis). Data for thin films produced using solutions containing either mixed

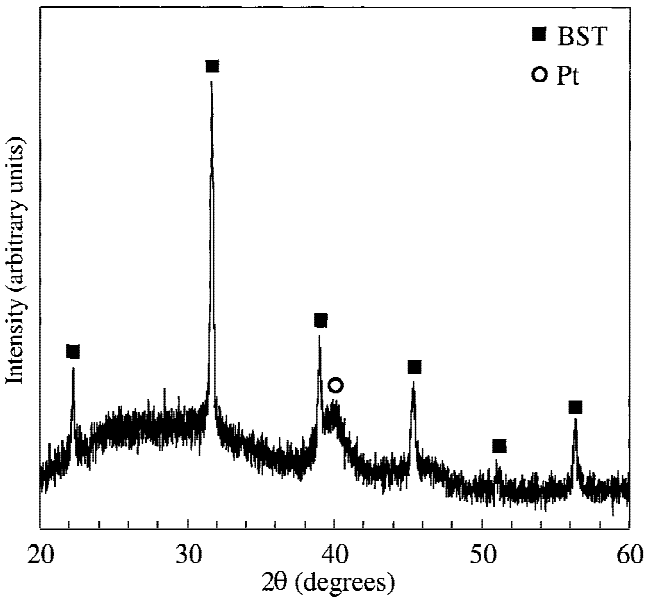

FIG. 2. XRD spectrum for a $Ba_{0.70}Sr_{0.30}TiO_3$ thin film processed at 90 °C for 36 h using an aqueous solution of 0.45 M $Ba(OH)_2$ and 0.05 M $Sr(OH)_2$.

TABLE I. WDS data for a $Ba_{0.50}Sr_{0.50}TiO_3$ thin film processed at 90 °C for 36 h in 0.50 M aqueous hydroxide solution containing a 75:25 molar ratio of Ba:Sr.

	Ba	Sr	Ti	Total
Weight %	12.4	7.4	8.3	28.1
Standard deviation (%)	0.22	0.21	0.38	. . .
Normalized atomic %	25.5	24.4	50.6	100.0

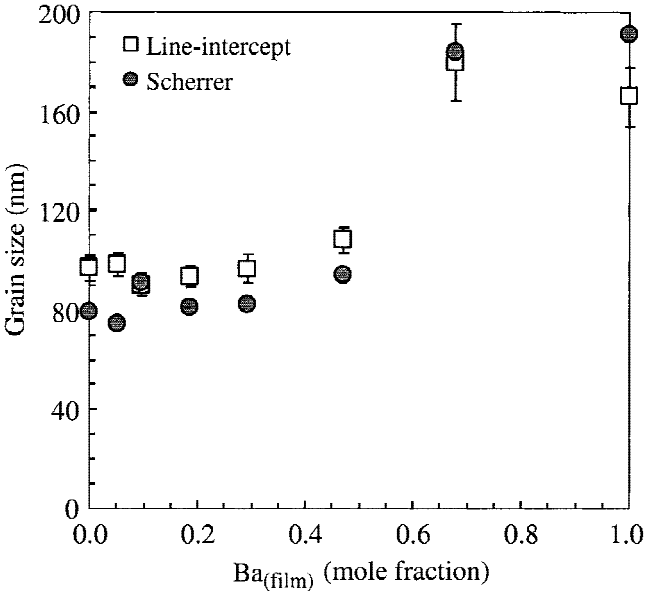

FIG. 3. Average grain size as a function of composition [*x* in $Ba_xSr_{(1-x)}TiO_3$] for BST thin films.

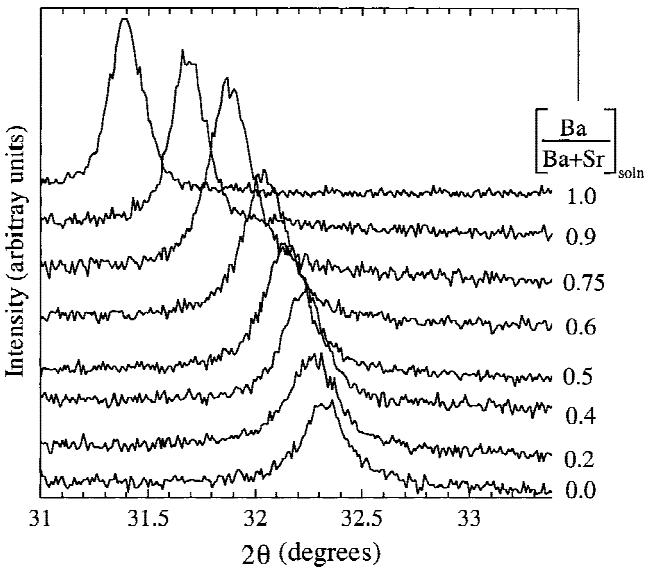

FIG. 4. XRD spectra showing the (110) peak for BST thin films processed at 90 °C for 36 h in solutions containing varying amounts of $Ba(OH)_2$ and $Sr(OH)_2$. The mole fraction of Ba^{2+} in solution is shown on the right.

chlorides or mixed hydroxides are shown in addition to the data for BST powders.[19] If the BST stoichiometries directly reflected the initial solution composition, the experimental data would follow a straight line of unit slope. Except for solutions containing only Ba^{2+} or only Sr^{2+}, the overall thin-film stoichiometry exhibited a preferential incorporation of Sr^{2+}, similar to the data previously reported for BST powders.[19] The results of this study were also in agreement with those of Kajiyoshi *et al.*[28] (Fig. 6), who processed BST thin films from a Ti metal precursor using an applied electric field at temperatures greater than 100 °C. These results imply that preferred Sr^{2+} incorporation appears to be a feature of the hydrothermal processing method and is independent of the sources of Ba, Sr, and Ti.

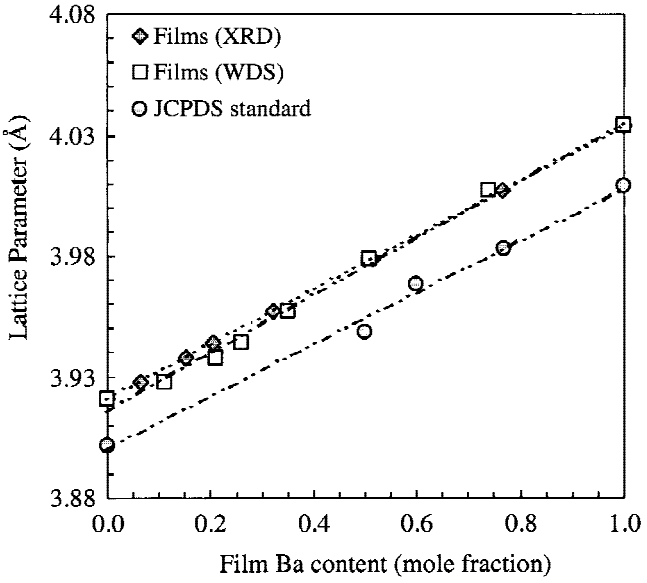

FIG. 5. Lattice parameter–composition calibration curve, showing Vegard's law is obeyed for hydrothermally derived BST thin films. The lattice parameter–composition calibration curve for JCPDS standards is shown for comparison. The cube root of a^2c is plotted for the JCPDS standards for which $x > 0.7$ in $Ba_xSr_{(1-x)}TiO_3$, since these BST solid solutions were tetragonal.

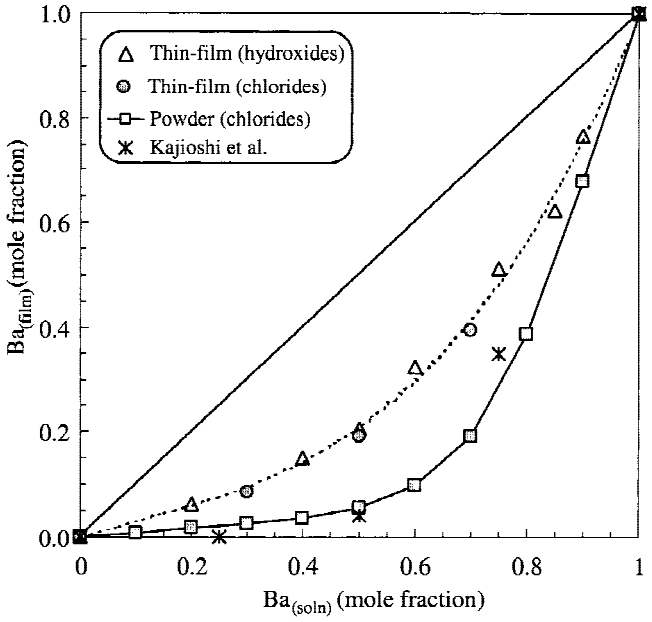

FIG. 6. Effects of the mole fraction of Ba^{2+} and Sr^{2+} initially in solution on the BST thin-film stoichiometry from lattice parameter measurements, showing the Ba^{2+} mole fraction (x in $Ba_xSr_{(1-x)}TiO_3$) in the thin film (y-axis) versus the Ba^{2+} mole fraction initially in solution (x-axis). The dashed line represents the best-fit curve through the BST thin films in this study. The thin-film data from Kajioshi *et al.*[28] and the BST powder data from Roeder and Slamovich[19] are shown for comparison.

B. Processing effects on dielectric properties

1. Dielectric constant and dielectric loss

The dielectric constant and dielectric loss of as-formed BST thin-films are shown in Fig. 7. The dielectric constant ranged from 100 to 185 and was highest for films with a Ba mole fraction of 0.35–0.75. The data are consistent with observations that the dielectric behavior of $Ba_xSr_{(1-x)}TiO_3$ depends on composition, although the dielectric constant of fine-grained BST films is considerably suppressed relative to bulk values for BST.[29–34] The dielectric loss varied little with composition, and tan δ ranged between 0.18 and 0.22. The error bars represent the scatter in dielectric data collected from five capacitors sampled at random across the film surface. The small scatter suggests that the films have a uniform thickness and microstructure. The dielectric constants for the films in this study are lower than generally observed for BST films produced using higher temperature methods. For example, values up to 580 have been reported for BST films of similar thickness produced by metalorganic

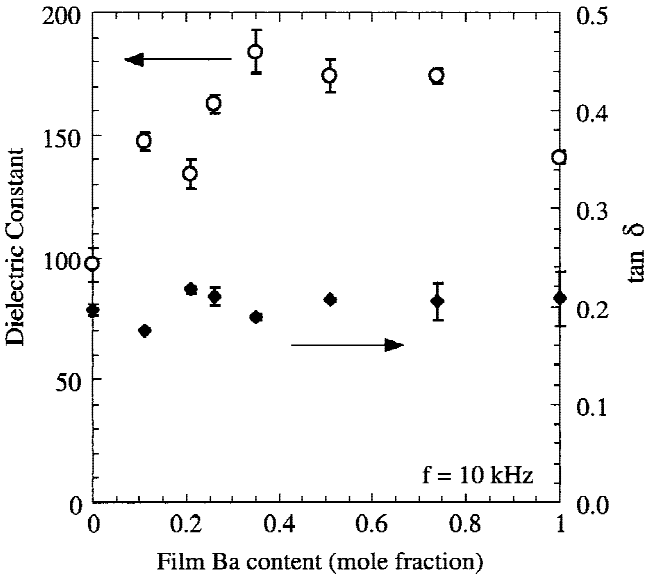

FIG. 7. Dielectric constant and dielectric loss as a function of composition for as-formed BST thin films measured at a frequency of 10 kHz.

decomposition.[34] Investigations of hydrothermally derived $BaTiO_3$ films by the reaction of titanium in solutions of $Ba(OH)_2$ at 180 °C have resulted in films with dielectric constants as high as 450.[35] Another study used a combination of electrochemical and hydrothermal processes to produce continuous $BaTiO_3$ films at 150 °C with a dielectric constant near 350.[36]

After heating of the BST films to perform measurements at temperatures up to 200 °C, it was observed that the dielectric constant and dielectric loss did not return to the same value as the as-formed films upon cooling to room temperature. In general, both the dielectric constant and dielectric loss values decreased by approximately 25–30%. This phenomenon has been observed by others.[26] The reduction in dielectric constant following annealing may be attributed to the reduction in ion jump polarization due to the expected decrease in the number of vacancy compensated hydroxyl ions (OH^-) on oxygen lattice sites following heating.[27] The time-lag of ion motion into vacant sites with respect to the applied ac field could contribute to the high dielectric losses observed in as-formed films. To avoid ambiguities associated with this effect, the films were heated in air to 200 °C for 30 min prior to measuring the *C–V* and *I–V* behavior discussed below. This was found to produce consistent measurements.

2. Capacitance–voltage behavior

The dielectric constant of BST depends on applied electric field.[8,37–40] Tunability, defined as $(\epsilon_{max} - \epsilon_{min})/\epsilon_{max}$, may be used to quantify this dependence for a given applied field and temperature. Commonly observed room-temperature tunabilities for $Ba_xSr_{(1-x)}TiO_3$ films formed by MOCVD or CSD methods for which $x = 0.6–0.8$ are within the range 15–25% for applied fields of 170 kV/cm.[41–43] The relationship between capacitance and applied voltage at room temperature was measured for $BaTiO_3$, BST, and $SrTiO_3$ thin films. The data are plotted in Fig. 8 using the geometry-independent variables dielectric constant verses applied electric field. The lower zero field dielectric constant at room temperature relative to the values reported for the as-formed films (Fig. 7) is a result of the 200 °C heat treatment. With an applied field of 170 kV/cm, films of $Ba_{0.70}Sr_{0.30}TiO_3$, $BaTiO_3$, and $Ba_{0.50}Sr_{0.50}TiO_3$ exhibited tunabilities of 8.4%, 8.1%, and 2.3%, respectively. Films with less than 0.30 mol fraction Ba^{2+} showed virtually no dependence of dielectric constant on applied field.

In 1962, Johnson derived an expression[44] for the electric field and temperature dependence of the dielectric constant on the basis of the theory of Devonshire:

$$\epsilon' = \frac{\epsilon'_0}{(1 + a\epsilon'^3_0 E^2)^{1/3}} \quad . \qquad (1)$$

Equation (1) is valid for bulk BST in the paraelectric state, where ϵ'_0 and ϵ' are values for the dielectric constant under zero bias field and under bias field E, respectively, and a is a coefficient which accounts for anharmonic ionic interactions. The solid lines in Fig. 8 were obtained by adjusting the anharmonic coefficient to fit Eq. (1). When the anharmonic coefficients of BST films of different compositions are compared, the value of the coefficient at (or near) the Curie temperature (T_C) should be used for a fair comparison. T_C for bulk $BaTiO_3$ is near 120 °C,[45] while T_C for $Ba_{0.70}Sr_{0.30}TiO_3$ is close to room temperature.[25,46] For films in this study, the value of a for $BaTiO_3$ and $Ba_{0.70}Sr_{0.30}TiO_3$ at their T_C values was 4.9×10^{18} and 5.6×10^{18} ($cm^2\ V^{-2}$), respectively. Values of a for $Ba_{0.50}Sr_{0.50}TiO_3$ and $SrTiO_3$ at their T_C values were not available because dielectric properties were not assessed below room temperature. The values for a follow the trend reported by Liou and Chiou,[46] who reported anharmonic coefficients for bulk BST. They attributed the increasing value of a with Sr content to the smaller ionic radius of Sr^{2+} relative to

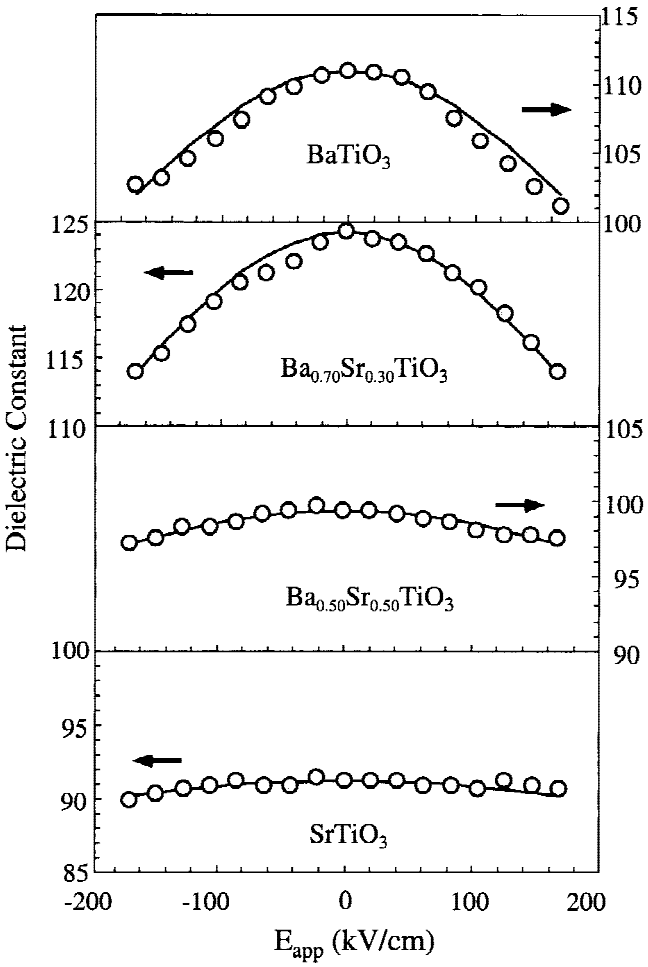

FIG. 8. Dielectric constant as a function of applied field for $BaTiO_3$, $Ba_{0.70}Sr_{0.30}TiO_3$, $Ba_{0.50}Sr_{0.50}TiO_3$, and $SrTiO_3$ thin films.

Ba^{2+}. They reasoned that the smaller Sr^{2+} ion contracts the unit cell, resulting in a shorter distance between the Ti^{4+} ion and its non-nearest neighbors, enhancing the anharmonic effect. The values reported by Liou and Chiou were 1 order of magnitude smaller than the anharmonic coefficient calculated for films in this study. Discrepancies may be due to the inherent difference between thin films and bulk materials (e.g. grain size, internal stress) and/or because much larger fields were applied to the films in this study for *C–V* characterization.

According to Eq. (1), the quantity (ϵ'/ϵ'_0) decreases as the zero-bias dielectric constant ϵ'_0 increases. Because ϵ'_0 is typically largest near the Curie temperature, the dielectric tunability should be largest (for a given composition) near T_C and should diminish as the measurement temperature deviates from T_C. Measurements of dielectric constant for $BaTiO_3$ and $Ba_{0.70}Sr_{0.30}TiO_3$ over the temperature range 25 to 150 °C showed very broad peaks near the expected T_C for bulk materials (Fig. 9). The 50:50 BST film shows a steady increase in dielectric constant with decreasing temperature. At room temperature and above, the dielectric constant of the Sr-rich films was relatively invariant with respect to temperature, since T_C for Sr-rich compositions (as determined for the bulk) is well below room temperature, reaching 42 K for $SrTiO_3$.[8] The variation in dielectric constant with temperature was reflected in the dielectric tunability. Measurements of tunability as a function of temperature at an applied field of 170 kV/cm exhibited the trend in dielectric behavior predicted by Eq. (1) (Fig. 10). The tunability for $BaTiO_3$ reached a peak value of 10.0% at 125 °C, and the tunability of the $Ba_{0.70}Sr_{0.30}TiO_3$ film increased as the measurement temperature decreased toward room temperature. The 50:50 BST and $SrTiO_3$ films also show trends similar to the dielectric constant versus temperature behavior.

3. Current–voltage behavior

Interpretation of the relationship between leakage current density and applied electric field (*I–V* curves) for BST thin films must be done with care, since slow

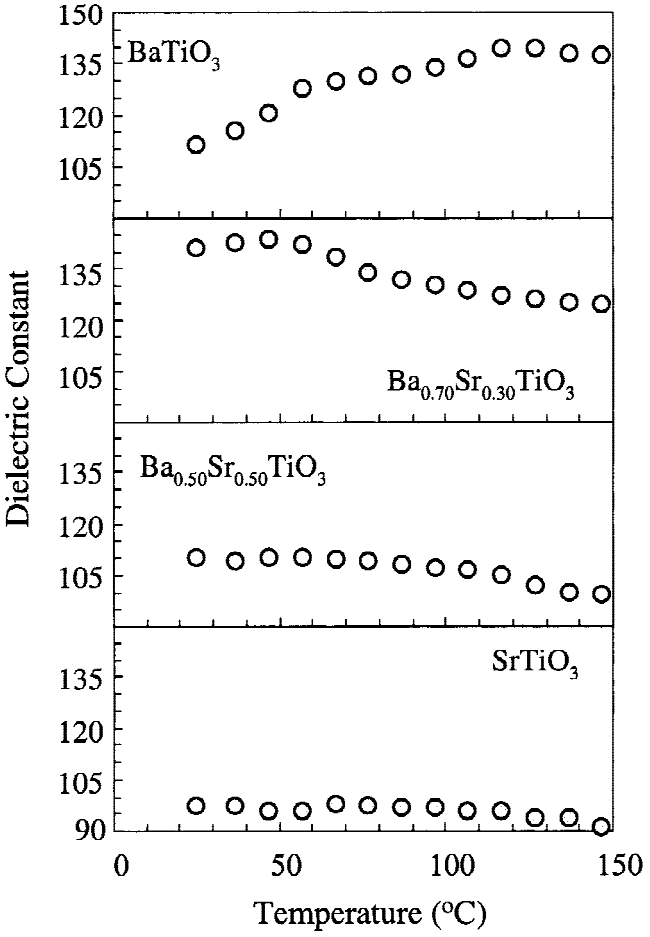

FIG. 9. Dielectric constant as a function of temperature for $BaTiO_3$, $Ba_{0.70}Sr_{0.30}TiO_3$, $Ba_{0.50}Sr_{0.50}TiO_3$, and $SrTiO_3$ thin films.

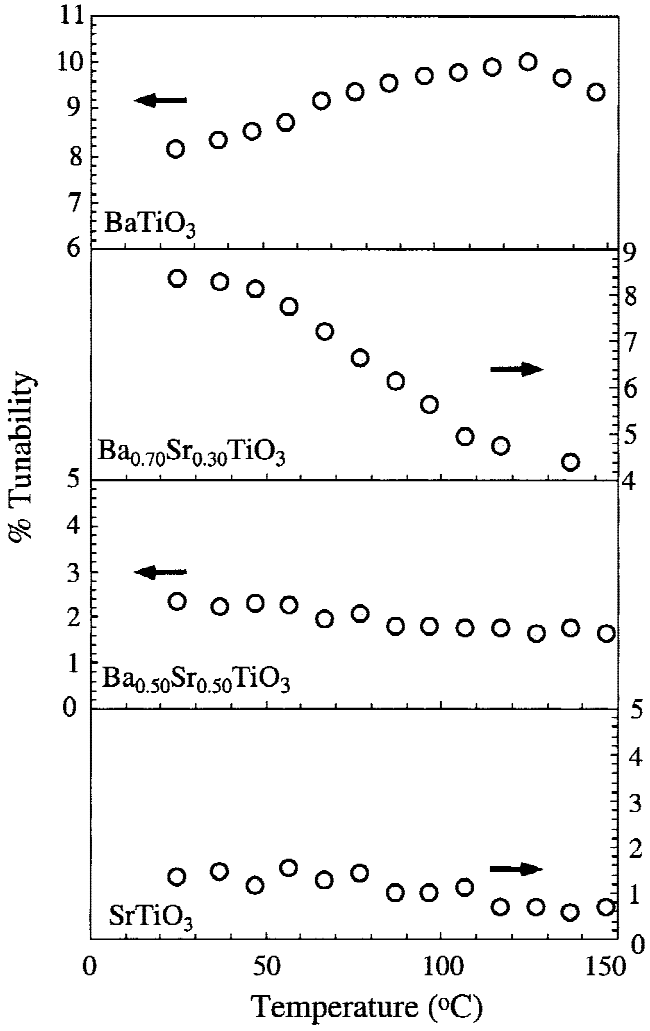

FIG. 10. Tunability at 170 kV/cm as a function of temperature for $BaTiO_3$, $Ba_{0.70}Sr_{0.30}TiO_3$, $Ba_{0.50}Sr_{0.50}TiO_3$, and $SrTiO_3$ thin films.

polarization currents can prevent observation of the true leakage behavior. Therefore, a voltage step measurement approach described by Dietz *et al.*[25] was used to separate the polarization and leakage currents. *I–V* data for $BaTiO_3$, $Ba_{0.50}Sr_{0.50}TiO_3$, and $SrTiO_3$ thin films are plotted on a log scale to amplify the transition in conduction from ohmic, below approximately 100 kV/cm, to conduction limited by thermionic emission of electrons at higher fields (Fig. 11).[25,48] The shapes of the *I–V* curves were not strongly dependent on composition, but the magnitude of the leakage decreased with Sr content in BST.

On the basis of the experimental results of Dietz *et al.* for $SrTiO_3$ and $Ba_{0.7}Sr_{0.3}TiO_3$ thin films, the most favored conduction mechanism is that of Schottky-barrier-limited current flow.[25] Kotecki *et al.* also observed this behavior for $Ba_{0.65}Sr_{0.35}TiO_3$ thin films deposited by MOCVD.[9] For this case, electronic conduction occurs when charge carriers are thermally excited over the potential energy barrier at the electrode–ceramic interface. The so-called Schottky effect causes a field-dependent lowering of the energy barrier, causing an increase in conduction with applied field. The temperature and field dependence for thermionic emission over a reverse-biased Schottky barrier is given by[25,48,49]

$$J = A^{**}T^2 \exp\left(\frac{-W_B}{k_b T}\right) \exp\left(\frac{q}{k_b T}\sqrt{\frac{q}{4\pi\epsilon_r}E}\right) \quad , \qquad (2)$$

where A^{**} is the effective Richardson constant (which incorporates carrier mobility), T is temperature, W_B is the zero-field barrier height, k_b is the Boltzmann constant, q is the electronic charge, E is the applied field, and ϵ_r is the dielectric constant. If the conduction mechanism is dominated by thermionic emission, plots of $\ln(J)$ versus $E^{0.50}$ and $\ln(J/T^2)$ versus $1/T$ (Schottky plots) yield straight lines. The barrier height, W_B, is then extracted from either the slopes or intercepts of the temperature- and field-dependent plots.[25,48] Schottky plots for the films in this study under positive applied fields yield a linear response for applied fields of 100 kV/cm and greater (Fig. 12), verifying Schottky-barrier-dominated conduction. The conduction behavior for negative applied fields yields similar results.

The barrier heights calculated using Eq. (2) are 0.56, 0.67, and 0.56 eV for $BaTiO_3$, $Ba_{0.50}Sr_{0.50}TiO_3$, and

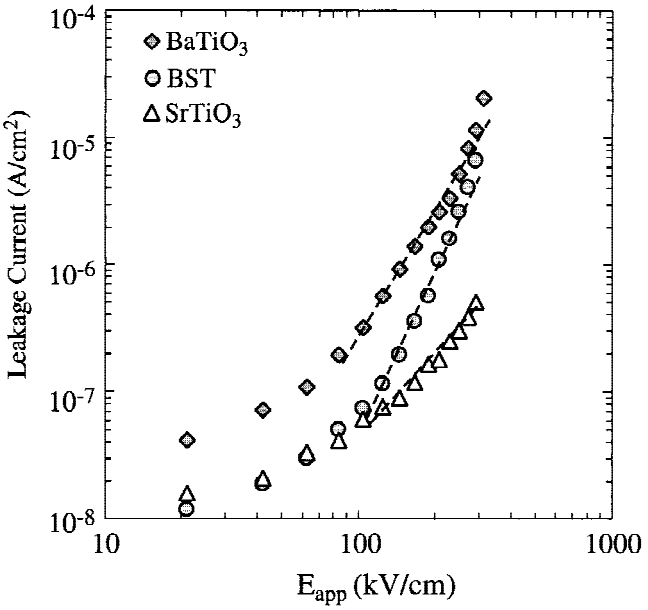

FIG. 11. Leakage current as a function of applied field for $BaTiO_3$, $Ba_{0.50}Sr_{0.50}TiO_3$, and $SrTiO_3$ thin films.

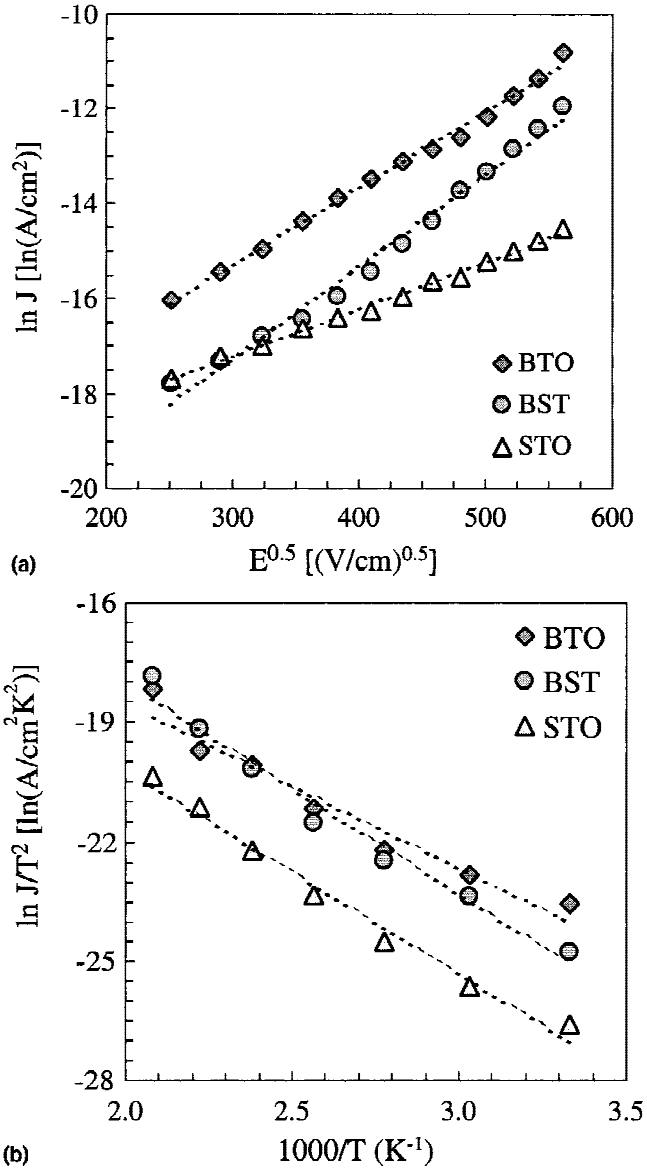

FIG. 12. Schottky plots showing (a) field dependence of leakage current at 25 °C and (b) temperature dependence of leakage behavior for an applied field of 250 kV/cm, based on the leakage current data for $BaTiO_3$, $Ba_{0.50}Sr_{0.50}TiO_3$, and $SrTiO_3$ thin films.

$SrTiO_3$ thin films, respectively. The nominal barrier height of the insulator–metal interface (assuming a fully depleted insulator layer[25]) is the difference between the metal work function and the electron affinity of the insulator ($W_B - q\chi$). The work function of Pt is 5.4 eV,[50] and the values of the electron affinity for $BaTiO_3$ and $SrTiO_3$ have been determined for bulk single crystals to be 2.5 [51] and 4.1 eV,[52] respectively. Thus, the ideal Pt/$BaTiO_3$ barrier height is 2.9 and 1.3 eV for Pt/$SrTiO_3$; the barrier height for Pt/BST is expected to be somewhere in between these values.

Kwak *et al.*[53] showed that the interface state density in BST thin films with Pt electrodes decreased by one-third following annealing in O_2 or N_2. They observed a corresponding decrease in the leakage current, indicating that interface trap density may play a role in determining the effective Schottky barrier height. Lower than expected barrier height values were observed by Kotecki *et al.*[9] and Baniecki *et al.*[54] for Pt/BST films deposited by MOCVD; however, they observed an increase in the barrier height from approximately 0.65 eV for as-deposited films to 1.2 eV following annealing in O_2 at 550 °C. Considering these results, the lower values obtained for the films in this study may result from a high density of interface states in the as-deposited films, although further studies are needed to determine the precise cause. Interface defect density, crystalline quality, amount of noncrystalline phase (if any), and grain size can each affect the interface state density and the corresponding barrier height.

Although Schottky-barrier-limited thermionic emission appears to be the dominant conduction mechanism for films in this study, cold field emission may also contribute to the total conduction. This temperature-independent mechanism has been observed in other perovskite thin-film systems, including $SrTiO_3$ at electric fields exceeding approximately 200 kV/cm,[48] and in $Pb(Zr,Ti)O_3$ over a wide range of electric fields.[55]

IV. CONCLUSIONS

The role of processing on phase stoichiometry was investigated for hydrothermally derived $Ba_xSr_{(1-x)}TiO_3$ thin films produced at 90 °C in alkaline solutions. Similar to studies of hydrothermally derived BST powders, the film stoichiometry deviated from solution composition, with a preferred incorporation of Sr^{2+}. The dielectric constant at 10 kHz depended on composition and ranged from 100 to 185, and the dielectric loss ranged from 0.18 to 0.22. Capacitance–voltage measurements showed the dependence of dielectric constant on applied field varied with Ba^{2+} content. In accordance with dielectric behavior predicted by Devonshire's theory, the $Ba_{0.70}Sr_{0.30}TiO_3$ film showed maximum tunability at room temperature, while the dielectric constant of films with less than 0.30 mol fraction Ba^{2+} was independent of applied field. Current–voltage measurements indicated the leakage current density decreased with Sr^{2+} content. Analysis of field- and temperature-dependent leakage current measurements suggested that Schottky-barrier-limited current flow was the dominant conduction mechanism for fields exceeding 100 kV/cm, regardless of composition. The metal/insulator barrier height was lower than expected, possibly due to a high density of interface states.

ACKNOWLEDGMENTS

The authors gratefully acknowledge the Earth and Atmospheric Science Department at Purdue University and C. Hager for assistance with WDS measurements. The authors also thank the National Science Foundation for supporting this research under Grant DMR-9623744.

REFERENCES

1. O. Auciello, Integr. Ferroelectr. **15,** 211 (1997).
2. J.F. Scott, Annu. Rev. Mater. Sci. **28,** 79 (1998).
3. D.M. Tahan, A. Safari, and L.C. Klein, J. Am. Ceram. Soc. **79,** 1593 (1996).
4. D. Hennings, Int. J. High Technol. Ceram. **3,** 91 (1987).
5. D.L. Polla and L.F. Francis, MRS Bull. July, 59 (1996).
6. H. Beratan, C. Hanson, and G. Meissner, SPIE Proc. **2274,** 147 (1994).
7. F. Jin, G.W. Auner, R. Naik, N.W. Schubring, J.V. Mantese, A.B. Catalan, and A.L. Micheli, Appl. Phys. Lett. **73,** 2838 (1998).
8. O.G. Vendik, E.K. Hollmann, A.B. Kozyrev, and A.M. Prudan, J. Supercond. **12,** 325 (1999).
9. D.E. Kotecki, J. Baniecki, H. Shen, R. Laibowitz, K. Saenger, J. Lian, T. Shaw, S. Athavale, C. Cabral, P. Duncombe, M. Gutsche, G. Kunkel, Y. Park, Y. Wang, and R. Wise, IBM J. Res. Develop. **43,** 367 (1999).
10. T. Yoshimura, N. Fujimura, and T. Ito, J. Cryst. Growth **174,** 790 (1997).
11. J.J. Xu, A.S. Shaikh, and R.W. Vest, IEEE Trans. Ultrason. Ferroelectr. Freq. Control **36,** 307 (1989).
12. R. Kullmer, Appl. Phys. A, **65,** 273 (1997).
13. H.B. Sharma and A. Mansingh, J. Phys. D: Appl. Phys. **31,** 1527 (1998).
14. M.M. Lencka and R.E. Riman, Chem. Mater. **5,** 61 (1993).
15. E.B. Slamovich and I.A. Aksay, in *Better Ceramics Through Chemistry VI,* edited by A.K. Cheetham, C.J. Brinker, M.L. Mecartney, and C. Sanchez. (Mater. Res. Soc. Symp. Proc. **346,** Pittsburgh, PA, 1994), p. 63–68.
16. R. Basca, P. Ravindranathan, and J. Dougherty, J. Mater. Res. **7,** 423 (1992).
17. J. Eckert, C. Hung-Houston, B. Gersten, M. Lencka, and R. Riman, J. Am. Ceram. Soc. **79,** 2929 (1996).
18. M. Yoshimura, W. Suchanek, T. Watanabe, and B. Sakurai, J. Mater. Res. **13,** 875 (1998).
19. R.K. Roeder and E.B. Slamovich, J. Am. Ceram. Soc. **82,** 1665 (1999).
20. A.S. Shaikh and G.M. Vest, J. Am. Ceram. Soc., **69,** 682 (1986).
21. R.K. Roeder and E.B. Slamovich, Ceram. Trans. **83,** 375 (1998).
22. R.K. Roeder and E.B. Slamovich, J. Mater. Res. **14,** 2364 (1999).
23. G.W. Dietz, W. Antpöhler, M. Klee, and R. Waser, J. Appl. Phys. **78,** 6113 (1995).

24. *Software manual for Siemens DIFFRAC-AT v.3.1 and Profile Fitting Program v.1.5* (Siemens Analytical X-Ray Instruments, Cherry Hill, NJ, 1988).
25. G.W. Dietz, M. Schumacher, R. Waser, S.K. Strieffer, C. Basceri, and A.I. Kingon, J. Appl. Phys. **82,** 2359 (1997).
26. A.T. Chien, X. Xu, J.H. Kim, J. Sachleben, J.S. Speck, and F.F. Lange, J. Mater. Res. **14,** 3330 (1999).
27. D. Hennings and S. Schreinemacher, J. Eur. Ceram. Soc. **9,** 41 (1992).
28. K. Kajiyoshi, M. Yoshimura, Y. Hamaji, K. Tomono, and T. Kasanami, J. Mater. Res. **11,** 169 (1996).
29. U. Syamaprasad, R.K. Galgali, and B.C. Mohanty, Mater. Lett. **8,** 36 (1989).
30. M.H. Frey, Z. Xu, P. Han, and D.A. Payne, Ferroelectrics **206–207,** 337 (1998).
31. M.S. Mohammed, R. Naik, J. Mantese, N. Schubring, A. Micheli, and A. Catalan, J. Mater. Res. **11,** 2588 (1996).
32. C.J. Peng and S.B. Krupanidhi, in *Proceedings of the 9th IEEE International Symposium on Applications of Ferroelectrics* (IEEE, Piscataway, NJ, 1994), p. 460.
33. Y. Kato, H. Yabuta, S. Sone, H. Yamaguchi, T. Iizuka, S. Yamamichi, P-Y. Lesaicherre, S. Nishimoto, and Y. Yoshida in *Ferroelectric Thin Films V*, edited by S.B. Desu, R. Ramesh, B.A. Tuttle, R.E. Jones, and I.K. Yoo. (Mater. Res. Soc. Symp. Proc. **433,** Pittsburgh, PA, 1996), p. 3–8.
34. S.B. Krupanidhi and C.J. Peng, Thin Solid Films **305,** 144 (1997).
35. R.R. Basca, J.P. Dougherty, and L.J. Pillone, Appl. Phys. Lett. **63,** 1053 (1993).
36. K. Kajiyoshi, Y. Sakabe, and M. Yoshimura, Jpn. J. Appl. Phys. **36,** 1209 (1997).
37. A. Outzourhit, U. Trefny, T. Kito, and B. Yarar, J. Mater. Res. **10,** 1411 (1995).
38. A. Outzourhit, J.U. Trefny, T. Kito, B. Yarar, A. Naziripur, and A.M. Hermann, Thin Solid Films **259,** 218 (1995).
39. J. Lindner, F. Weiss, J.P. Senateur, V. Galindo, W. Haessler, M. Weihnacht, J. Santiso, and A. Figueras, J. Eur. Ceram. Soc. **19,** 1435 (1999).
40. S. Sengupta, D.P. Vijay, and S.B. Desu, in *Ferroelectric Thin Films IV*, edited by S.B. Desu, B.A. Tuttle, R. Ramesh, and T. Shiosaki (Mater. Res. Soc. Symp. Proc. **361,** Pittsburgh, PA, 1995), p. 545–550.
41. C. Basceri, S.K. Streiffer, A.I. Kingon, and R. Waser, J. Appl. Phys. **82,** 2497 (1997).
42. J. Kim, S. Kwun, and J. Yoon, in *Proceedings of the 9th IEEE International Symposium on Applications of Ferroelectrics* (IEEE, Piscataway, NJ, 1994), p. 422.
43. D. Tahan, A. Safari, and L.C. Klein, in *Proceedings of the 9th IEEE International Symposium on Applications of Ferroelectrics* (IEEE, Piscataway, NJ, 1994), p. 427.
44. K.M. Johnson, J. Appl. Phys. **33,** 2826 (1962).
45. W.J. Merz, Phys. Rev. **76,** 1221 (1949).
46. J. Liou and B. Chiou, J. Am. Ceram. Soc. **80,** 3093 (1997).
47. H.T. Martirena and J.C. Burfoot, J. Phys. C: Solid State Phys. **7,** 3182 (1974).
48. G.W. Dietz and R. Waser, Thin Solid Films **299,** 53 (1997).
49. S.M. Sze, *Physics of Semiconductor Devices* (John Wiley & Sons, Inc., New York, 1969).
50. V.S. Formenko, *Handbook of Thermionic Properties*, edited by G.V. Samsonov (Plenum Press Data Division, New York, 1966).
51. L. Hafid, G. Godefroy, A. El Idrissi, and F. Michel-Calendini, Solid State Commun. **66,** 841 (1988).
52. V.E. Henrich, G. Dresselhaus, and H.J. Zeiger, Phys. Rev. B **17,** 4908 (1978).
53. D.H. Kwak, B.T. Jang, S.Y. Cha, J.S. Lee, and H.C. Lee, Integr. Ferroelectr. **17,** 179 (1997).
54. J.D. Baniecki, R.B. Laibowitz, T.M. Shaw, K.L. Saenger, P.R. Duncombe, C. Cabral, D.E. Kotecki, H. Shen, J. Lian, and Q.Y. Ma, J. Eur. Ceram. Soc. **19,** 1457 (1999).
55. I. Stolichnov, A.K. Tagantsev, E.L. Colla, and N. Setter, Appl. Phys. Lett. **73,** 1361 (1998).